Low-Thrust Control of Constellations Using Artificial Potential Function for Multipoint Emergency Observation

Fang Zhengqing[1], Liu Fucheng[2], Wang Zhaokui[3]

[1] School of Aerospace Engineering, Tsinghua University
Beijing, China
Phone: +86 010-62794316, Mail: fzq22@mails.tsinghua.edu.cn wangzk@mail.tsinghua.edu.cn

[2] Shanghai Academy of Spaceflight Technology
Shanghai, China
Phone: +86 021-24183423, Mail: lfczrjj@163.com

Abstract: With the advancement of satellite remote sensing technologies, constellations are now employed as monitoring agents for designated areas. Nevertheless, multiple emergencies may occur at the same time around the globe. This paper focuses on constellation configuration control strategy for multipoint observation. Artificial potential function (APF) control method is adopted to solve the autonomous continuous low-thrust reconfiguration control problem. Extended orbital elements were employed to construct the quadratic potential function. Lyapunov stability of the proposed algorithm was proved. In addition, a repulsive potential function using relative distance was developed for collision avoidance. Simulations were carried out for testing various missions to validate the proposed APF-based control method, and the results indicate that the proposed control strategy is efficient, stable, and fulfills the demand for simultaneous multipoint emergency observation.

1. INTRODUCTION

A satellite constellation is a typical distributed space system. With the advancement of satellite remote sensing technologies, constellations are now employed as monitoring agents for designated areas. Individual satellites with maneuvering capability in the constellation can provide frequent overflights and coverages to the region of interest. Nevertheless, multiple emergencies may occur at the same time around the globe. For a monitoring constellation, as a result, the capability of simultaneous multipoint monitoring is required. The constellation will need the ability of autonomous collaborative formation, reconfiguration, and maintenance. Individual satellites in mega-constellations launched recently are mostly equipped with continuous low-thrust systems, such as electric propulsion, in which the methods of impulse control for satellite formation and mission planning can longer be applied. A novel method of constellation formation control using continuous low thrust for simultaneous multipoint observation is urgently demanded.

Artificial potential function (APF) method has shown its potential for constellation configuration control. In a paper by Xu et al. [1][2], relative orbital elements-based APF control was employed for reconfiguration, bounded flight, and collision avoidance for satellite clusters. Autonomous replacement and deorbiting for constellations using classical orbital elements-based APF control [3] was also accomplished. Yu et al. investigated distributed autonomous low-thrust APF control methods for satellite cluster long-distance gathering [4]. In present paper, a constellation configuration APF control method for multipoint emergency observation is proposed.

2. METHODOLOGY

2.1 Dynamical model

For near-circular orbits, e can be close to 0, numerical singularities may happen in terms $\mathrm{d}\omega/\mathrm{d}t, \mathrm{d}M/\mathrm{d}t$ in Gauss equations. Therefore, extended orbital elements $a, \xi = e\cos\omega, \eta = e\sin\omega, i, \Omega, \lambda = M + \omega$ are introduced, Gauss equations can be rewritten as,

$$\begin{cases} \dfrac{\mathrm{d}a}{\mathrm{d}t} = \dfrac{2\sqrt{1+2e\cos f+e^2}}{n\sqrt{1-e^2}}U \\ \dfrac{\mathrm{d}\xi}{\mathrm{d}t} = \dfrac{\sqrt{1-e^2}}{na\sqrt{1+2e\cos f+e^2}}\left\{2(\cos u+e\cos\omega)U-\left[\sqrt{1-e^2}\sin E\cos\omega+(\cos E+e)\sin\omega\right]N\right\}+\eta\cos i\dfrac{\mathrm{d}\Omega}{\mathrm{d}t} \\ \dfrac{\mathrm{d}\eta}{\mathrm{d}t} = \dfrac{\sqrt{1-e^2}}{na\sqrt{1+2e\cos f+e^2}}\left\{2(\sin u+e\sin\omega)U-\left[\sqrt{1-e^2}\sin E\sin\omega-(\cos E+e)\cos\omega\right]N\right\}-\xi\cos i\dfrac{\mathrm{d}\Omega}{\mathrm{d}t} \\ \dfrac{\mathrm{d}i}{\mathrm{d}t} = \dfrac{r\cos u}{na^2\sqrt{1-e^2}}W \\ \dfrac{\mathrm{d}\Omega}{\mathrm{d}t} = \dfrac{r\sin u}{na^2\sqrt{1-e^2}\sin i}W \\ \dfrac{\mathrm{d}\lambda}{\mathrm{d}t} = n+\dfrac{\sqrt{1-e^2}}{na\sqrt{1+2e\cos f+e^2}}\left\{\left[\dfrac{2e\sin f}{1+\sqrt{1-e^2}}-2e\sin E\right]U+\left[\dfrac{e\cos E}{1+\sqrt{1-e^2}}+\left(1+\sqrt{1-e^2}\right)\right]N\right\}-\cos i\dfrac{\mathrm{d}\Omega}{\mathrm{d}t} \end{cases} \tag{1}$$

where a is the semi-major axis, e is the eccentricity, i is the inclination, ω is the right ascension of ascending node, Ω is the argument of perigee, M is the mean anomaly, μ is the geocentric gravitational constant, r is the geocentric distance of satellite, p is the semi-latus rectum, f is the true anomaly, E is the eccentricity anomaly, u is the argument of latitude, U, N, W are the components of the thrust acceleration vector in the tangential, principal normal and out-of-plane reference frame ($Ox_2y_2z_2$), shown as Fig1.b.

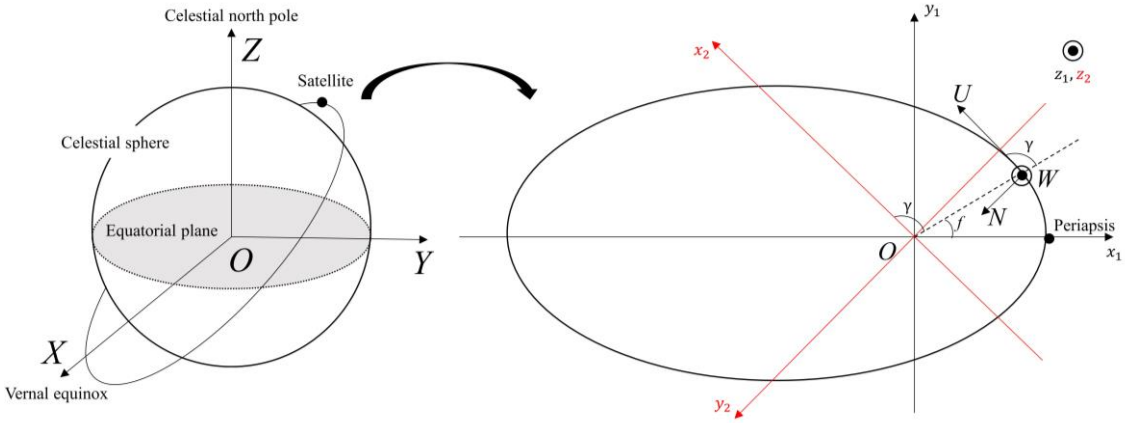

(a) Earth-centered inertial (ECI) reference frame (OXYZ)

(b) Tangential, principal normal and out-of-plane reference frame ($Ox_2y_2z_2$)

Fig1 Coordinate Systems

The transformation between the ECI frame $OXYZ$ and $Ox_2y_2z_2$ can be written as:

$$\{\mathbf{r},\mathbf{v}\}_{OXYZ} = \begin{bmatrix}\cos\Omega & -\sin\Omega & 0\\ \sin\Omega & \cos\Omega & 0\\ 0 & 0 & 1\end{bmatrix}\begin{bmatrix}1 & 0 & 0\\ 0 & \cos i & -\sin i\\ 0 & \sin i & \cos i\end{bmatrix}\begin{bmatrix}\cos(u+\gamma) & -\sin(u+\gamma) & 0\\ \sin(u+\gamma) & \cos(u+\gamma) & 0\\ 0 & 0 & 1\end{bmatrix}\{\mathbf{r},\mathbf{v}\}_{Ox_2y_2z_2} = A_{OXYZ\to Ox_2y_2z_2}\{\mathbf{r},\mathbf{v}\}_{Ox_2y_2z_2} \tag{2}$$

where $\sin\gamma = \mu(1+e\cos f)/hv, \cos\gamma = \mu e\sin f/hv$. The perturbing gravitational acceleration due to J_2 in $Ox_2y_2z_2$ is given by:

$$\left\{\mathbf{a}_{J_2}\right\}_{Ox_2y_2z_2}=-\frac{3}{2}\frac{\mu}{r^2}J_2\left(\frac{R_e}{r}\right)^2\begin{bmatrix}\cos\gamma\left(1-3\sin^2 i\sin^2 u\right)+\sin\gamma\sin^2 i\sin 2u\\-\sin\gamma\left(1-3\sin^2 i\sin^2 u\right)+\cos\gamma\sin^2 i\sin 2u\\\sin 2i\sin u\end{bmatrix} \tag{3}$$

2.2 Artificial potential function for reconfiguration control

2.2.1 Establishment of reconfiguration artificial potential function

The reconfiguration artificial potential function (APF) ϕ is given in the quadratic form. It contains two parts where ϕ_{slow} is based on slow variables and a,ξ,η,i,Ω and ϕ_{fast} is based on fast variable λ,

$$\begin{aligned}\phi_{\text{slow}}&=\frac{1}{2}k_a\left(\boldsymbol{\tau}_{\text{slow}}-\boldsymbol{\tau}_{\mathbf{t},\text{slow}}\right)^{\mathrm{T}}\mathbf{Q}_{\mathbf{a},\text{slow}}\left(\boldsymbol{\tau}_{\text{slow}}-\boldsymbol{\tau}_{\mathbf{t},\text{slow}}\right)\\\phi_{\text{fast}}&=\frac{1}{2}k_a\left(\boldsymbol{\tau}_{\text{fast}}-\boldsymbol{\tau}_{\mathbf{t},\text{fast}}\right)^{\mathrm{T}}\mathbf{Q}_{\mathbf{a},\text{fast}}\left(\boldsymbol{\tau}_{\text{fast}}-\boldsymbol{\tau}_{\mathbf{t},\text{fast}}\right)\\\phi&=\phi_{\text{slow}}+\phi_{\text{fast}}\end{aligned} \tag{4}$$

where $\boldsymbol{\tau}_{\text{slow}}=\left[a\ \ e\cos\omega\ \ e\sin\omega\ \ \cos i\ \ \sin i\ \ \cos\Omega\ \ \sin\Omega\right]^{\mathrm{T}}$, $\boldsymbol{\tau}_{\text{fast}}=\left[\cos\lambda\ \ \sin\lambda\right]^{\mathrm{T}}$ are the slow and fast state vectors of the controlled satellite, $\boldsymbol{\tau}_{\mathbf{t},\text{slow}},\boldsymbol{\tau}_{\mathbf{t},\text{fast}}$ are the state vectors of a target position, $\mathbf{Q}_{\mathbf{a},\text{slow}}=\text{diag}\left\{q_1,...,q_7\right\}$ and $\mathbf{Q}_{\mathbf{a},\text{fast}}=\text{diag}\left\{q_8,q_9\right\}$ are the weight matrices, k_a is the control coefficient. The low-thrust control $[\mathbf{u}]_{OXYZ}$ can be obtained by solving the partial differential of the APF to the velocity in the earth-centered inertial (ECI) system.

$$[\mathbf{u}]_{OXYZ}=A^{-1}_{OXYZ\to Ox_2y_2z_2}\begin{bmatrix}U\\N\\W\end{bmatrix}=-\begin{bmatrix}\frac{\partial\phi}{\partial\dot{X}}\\\frac{\partial\phi}{\partial\dot{Y}}\\\frac{\partial\phi}{\partial\dot{Z}}\end{bmatrix}=-\begin{bmatrix}\sum_j\frac{\partial\phi}{\partial C_j}\frac{\partial C_j}{\partial\dot{X}}\\\sum_j\frac{\partial\phi}{\partial C_j}\frac{\partial C_j}{\partial\dot{Y}}\\\sum_j\frac{\partial\phi}{\partial C_j}\frac{\partial C_j}{\partial\dot{Z}}\end{bmatrix} \tag{5}$$

where $[C_1,...,C_6]=[a,\xi,\eta,i,\Omega,\lambda]$ are the extended orbital elements. Consider the two-body equation of relative motion:

$$\ddot{\vec{r}}=-\frac{\mu}{r^2}\left(\frac{\vec{r}}{r}\right) \tag{6}$$

Let φ be an integral form of two-body motion which satisfies $\varphi\left(C_1,...,C_6\right)=\psi\left(\vec{r},\dot{\vec{r}}\right)$,Then the time derivative of φ is [5]:

$$\frac{\mathrm{d}\varphi}{\mathrm{d}t}=\frac{\partial\varphi}{\partial t}=\frac{\partial\psi}{\partial\vec{r}}\dot{\vec{r}}+\frac{\partial\psi}{\partial\dot{\vec{r}}}\ddot{\vec{r}}=\frac{\partial\psi}{\partial\vec{r}}\dot{\vec{r}}+\frac{\partial\psi}{\partial\dot{\vec{r}}}\vec{F}_0 \tag{7}$$

Suppose $\vec{F}_\epsilon$ is the perturbation acceleration, then the derivative of integral form of perturbed motion φ_P is:

$$\frac{\mathrm{d}\varphi_P}{\mathrm{d}t}=\frac{\partial\varphi}{\partial t}+\sum_j\frac{\partial\varphi}{\partial C_j}\dot{C}_j=\frac{\partial\psi}{\partial\vec{r}}\dot{\vec{r}}+\frac{\partial\psi}{\partial\dot{\vec{r}}}\left(\vec{F}_0+\vec{F}_\epsilon\right) \tag{8}$$

Combining Eq.(7) and Eq.(8), and let $\varphi_P = C_j$, then we have:

$$\frac{\partial C_j}{\partial \dot{\vec{r}}} \vec{F}_\epsilon = \frac{\mathrm{d}C_j}{\mathrm{d}t} \tag{9}$$

which means $\partial C_j / \partial \dot{\vec{r}}$ are coefficients of the *U*, *N*, *W* in Eqs.(1). Abbreviate Eqs.(1) as:

$$\begin{cases} \dfrac{\mathrm{d}a}{\mathrm{d}t} = b_1 U \\ \dfrac{\mathrm{d}\xi}{\mathrm{d}t} = b_2 U + b_3 N + b_4 W \\ \dfrac{\mathrm{d}\eta}{\mathrm{d}t} = b_5 U + b_6 N + b_7 W \\ \dfrac{\mathrm{d}i}{\mathrm{d}t} = b_8 W \\ \dfrac{\mathrm{d}\Omega}{\mathrm{d}t} = b_9 W \\ \dfrac{\mathrm{d}\lambda}{\mathrm{d}t} = n + b_{10} U + b_{11} N + b_{12} W \end{cases} \tag{10}$$

Therefore, the control can be given as,

$$\begin{bmatrix} U_{\text{slow}} \\ N_{\text{slow}} \\ W_{\text{slow}} \end{bmatrix} = -k_a \begin{bmatrix} b_1 \dfrac{\partial \phi}{\partial a} + b_2 \dfrac{\partial \phi}{\partial \xi} + b_5 \dfrac{\partial \phi}{\partial \eta} \\ b_3 \dfrac{\partial \phi}{\partial \xi} + b_6 \dfrac{\partial \phi}{\partial \eta} \\ b_4 \dfrac{\partial \phi}{\partial \xi} + b_7 \dfrac{\partial \phi}{\partial \eta} + b_8 \dfrac{\partial \phi}{\partial i} + b_9 \dfrac{\partial \phi}{\partial \Omega} \end{bmatrix}, \begin{bmatrix} U_{\text{fast}} \\ N_{\text{fast}} \\ W_{\text{fast}} \end{bmatrix} = -k_a \begin{bmatrix} b_{10} \dfrac{\partial \phi}{\partial \lambda} \\ b_{11} \dfrac{\partial \phi}{\partial \lambda} \\ b_{12} \dfrac{\partial \phi}{\partial \lambda} \end{bmatrix}, \begin{bmatrix} U \\ N \\ W \end{bmatrix} = \begin{bmatrix} U_{\text{fast}} + U_{\text{slow}} \\ N_{\text{fast}} + N_{\text{slow}} \\ W_{\text{fast}} + W_{\text{slow}} \end{bmatrix} \tag{11}$$

2.2.2 Stability

Lyapunov's second method is employed to examine the stability of the proposed reconfiguration potential function. A system $\dot{\mathbf{T}} = f(\mathbf{T}), f(\mathbf{0}) = \mathbf{0}$ can be proved stable if the Lyapunov function *V* satisfies the following conditions,

$$\begin{cases} V(\mathbf{0}) = 0, & & (a) \\ V(\mathbf{T}) > 0, & \forall \mathbf{T} \neq \mathbf{0} & (b) \\ \dot{V}(\mathbf{0}) = 0, & & (c) \\ \dot{V}(\mathbf{T}) \leq 0, \dot{V}(\mathbf{T}) \not\equiv 0 & \forall \mathbf{T} \neq \mathbf{0} & (d) \end{cases} \tag{12}$$

Considering $\mathbf{T} = \boldsymbol{\tau}_{\text{slow}} - \boldsymbol{\tau}_{\mathbf{t},\text{slow}}, V(\mathbf{T}) = \phi_{\text{slow}}(\mathbf{T})$, it satisfies (a)(b)(c) in Eq.(12). It can be proved that,

$$\begin{aligned} \dot{V}(\mathbf{T}) &= \frac{\partial V}{\partial \left(\boldsymbol{\tau}_{\text{slow}} - \boldsymbol{\tau}_{\mathbf{t},\text{slow}} \right)} \frac{\partial \left(\boldsymbol{\tau}_{\text{slow}} - \boldsymbol{\tau}_{\mathbf{t},\text{slow}} \right)}{\partial t} \\ &= -k_a \left[b_1 \left(\frac{\partial \phi_{\text{slow}}}{\partial a} \right) + b_2 \left(\frac{\partial \phi_{\text{slow}}}{\partial \xi} \right) + b_5 \left(\frac{\partial \phi_{\text{slow}}}{\partial \eta} \right) \right]^2 - k_a \left[b_3 \left(\frac{\partial \phi_{\text{slow}}}{\partial \xi} \right) + b_6 \left(\frac{\partial \phi_{\text{slow}}}{\partial \eta} \right) \right]^2 \\ &\quad -k_a \left[b_4 \left(\frac{\partial \phi_{\text{slow}}}{\partial \xi} \right) + b_7 \left(\frac{\partial \phi_{\text{slow}}}{\partial \eta} \right) + b_8 \left(\frac{\partial \phi_{\text{slow}}}{\partial i} \right) + b_9 \left(\frac{\partial \phi_{\text{slow}}}{\partial \Omega} \right) \right]^2 \leq 0 \end{aligned} \tag{13}$$

which means that the slow variable control is stable.

If we take fast variable λ into consideration, then we have:

$$
\begin{aligned}
\frac{\mathrm{d}V}{\mathrm{d}t} &= \frac{\partial V}{\partial \boldsymbol{\tau}}\frac{\mathrm{d}\boldsymbol{\tau}}{\mathrm{d}t} + \frac{\partial V}{\partial \boldsymbol{\tau}_t}\frac{\mathrm{d}\boldsymbol{\tau}_t}{\mathrm{d}t} \\
&= \frac{\partial V}{\partial \boldsymbol{\tau}}\left[\left.\frac{\mathrm{d}\boldsymbol{\tau}}{\mathrm{d}t}\right|_{two-body} + \frac{\partial \boldsymbol{\tau}}{\partial [\mathbf{v}]_{OXYZ}}[\mathbf{u}]_{OXYZ}\right] + \left.\frac{\partial V}{\partial \boldsymbol{\tau}_t}\frac{\mathrm{d}\boldsymbol{\tau}_t}{\mathrm{d}t}\right|_{two-body} \\
&= \left.\frac{\partial V}{\partial \boldsymbol{\tau}}\frac{\mathrm{d}\boldsymbol{\tau}}{\mathrm{d}t}\right|_{two-body} + \left.\frac{\partial V}{\partial \boldsymbol{\tau}_t}\frac{\mathrm{d}\boldsymbol{\tau}_t}{\mathrm{d}t}\right|_{two-body} - \left[\frac{\partial V}{\partial \boldsymbol{\tau}}\right]^2\left[\frac{\partial \boldsymbol{\tau}}{\partial [\mathbf{v}]_{OXYZ}}\right]^2 \\
&= -\left[\frac{\partial V}{\partial \boldsymbol{\tau}}\right]^2\left[\frac{\partial \boldsymbol{\tau}}{\partial [\mathbf{v}]_{OXYZ}}\right]^2 + k_a \mathbf{Q}_{\mathbf{a}}(\boldsymbol{\tau}-\boldsymbol{\tau}_t)\left.\left(\frac{\mathrm{d}\boldsymbol{\tau}}{\mathrm{d}t} - \frac{\mathrm{d}\boldsymbol{\tau}_t}{\mathrm{d}t}\right)\right|_{two-body}
\end{aligned}
\tag{14}
$$

Here:

$$
\frac{\mathrm{d}[\mathbf{v}]_{OXYZ}}{\mathrm{d}t} = -\mu\frac{[\mathbf{r}]_{OXYZ}}{r^3} + [\mathbf{u}]_{OXYZ}
\tag{15}
$$

$$
\frac{\mathrm{d}\boldsymbol{\tau}}{\mathrm{d}t} = \frac{\partial \boldsymbol{\tau}}{\partial [\mathbf{r}]_{OXYZ}}\frac{\mathrm{d}[\mathbf{r}]_{OXYZ}}{\mathrm{d}t} + \frac{\partial \boldsymbol{\tau}}{\partial [\mathbf{v}]_{OXYZ}}\frac{\mathrm{d}[\mathbf{v}]_{OXYZ}}{\mathrm{d}t} = \left.\frac{\mathrm{d}\boldsymbol{\tau}}{\mathrm{d}t}\right|_{two-body} + \frac{\partial \boldsymbol{\tau}}{\partial [\mathbf{v}]_{OXYZ}}[\mathbf{u}]_{OXYZ}
$$

According to Eq.(14), dV/dt is constantly negative when:

$$
\text{when } \left.\left(\frac{\mathrm{d}\boldsymbol{\tau}}{\mathrm{d}t} - \frac{\mathrm{d}\boldsymbol{\tau}_t}{\mathrm{d}t}\right)\right|_{two-body} = 0\ ,\ \frac{\mathrm{d}V}{\mathrm{d}t} = -\left[\frac{\partial V}{\partial \boldsymbol{\tau}}\right]^2\left[\frac{\partial \boldsymbol{\tau}}{\partial [\mathbf{v}]_{OXYZ}}\right]^2 < 0
\tag{16}
$$

which means the APF control method is Lyapunov stable when the rate of change of the controlled satellite state variables $\mathrm{d}\boldsymbol{\tau}/\mathrm{d}t$ under two-body gravity should be equal to that of the target satellite $\mathrm{d}\boldsymbol{\tau}_t/\mathrm{d}t$. Otherwise, convergence problems may occur.

2.3 Artificial potential function for collision avoidance

Additionally, as close encounters may occur during constellation reconfiguration between member satellites, a Gauss repulsive potential function between satellite *i* and *j* using relative distance is developed,

$$
\phi_{r,ij} = \frac{1}{2}\xi_{d_r}\exp\left[-\frac{\left(d_{ij}-d_{safe}\right)^2}{\sigma_{d_r}}\right],\ \text{if } d_{ij} \le d_{sight},\ i, j \in swarm
\tag{17}
$$

where d_{ij} is the distance between two satellites, d_{safe} is the target safe distance, ξ_{d_r} and σ_{d_r} are control coefficients. In the circumstance of *m* satellites, the repulsive control on satellite *i* is,

$$
\left\{\mathbf{a}_{i,\mathrm{rep}}\right\}_{OXYZ} = -\sum_{j=1}^{m}\nabla\phi_{r,ij} = -\sum_{j=1}^{m}\left(\frac{\partial\phi_{r,ij}}{\partial d_{ij}}\frac{\partial d_{ij}}{\partial X_i}\right)\vec{\mathbf{i}} - \sum_{j=1}^{m}\left(\frac{\partial\phi_{r,ij}}{\partial d_{ij}}\frac{\partial d_{ij}}{\partial Y_i}\right)\vec{\mathbf{j}} - \sum_{j=1}^{m}\left(\frac{\partial\phi_{r,ij}}{\partial d_{ij}}\frac{\partial d_{ij}}{\partial Z_i}\right)\vec{\mathbf{k}}
\tag{18}
$$

where $\vec{\mathbf{i}}$, $\vec{\mathbf{j}}$, $\vec{\mathbf{k}}$ are unit direction vectors in the ECI system. The repulsive control acceleration need to be transformed to the O$x_2y_2z_2$ system according to Eq. (2).

3. RESULTS

3.1 Single-satellite initialization

A simulation for case of a single-satellite was carried out in this section. The initial orbital elements of the controlled satellite were

$[a,e,i,\Omega,\omega,M]=[7528.14\text{km},10^{-4},53^{\circ},120^{\circ},0.01^{\circ},-50^{\circ}]$, the target orbital elements were $[a_t,e_t,i_t,\Omega_t,\omega_t,M_t]=[7578.14\text{km},10^{-4},53.8^{\circ},120^{\circ},0.01^{\circ},0^{\circ}]$. The reconfiguration coefficients were $k_a=5\times10^{-12}, Q_a=\text{diag}\{1.4\ \ 9.2e12\ 9.2e12\ 5e12\ 5e12\ 1e13\ 1e13\ 2e8\ 2e8\}$, repulsive coefficients were $d_{\text{safe}}=25e3, d_{\text{sight}}=500e3, \sigma=625e6, \xi_{d_r}=1$. The mass of the satellite was 225kg, the maximum thrust of the satellite was *F*=0.1N, and the specific impulse was *Isp*=3000s, which is also the same in simulations discussed in sections 3.2 and 3.3. The controlled trajectory in the geocentric inertial frame is presented in Fig.2a. The control acceleration plotted in Fig.2b. The difference between the controlled orbital elements and target values, i.e., control errors changing with time is presented in Fig.2c. In the simulation, in 5 days, all orbital elements converged to target values. The total fuel consumption was 1.16kg, while the controlled satellite moored at a safe distance of 28.4km from the target.

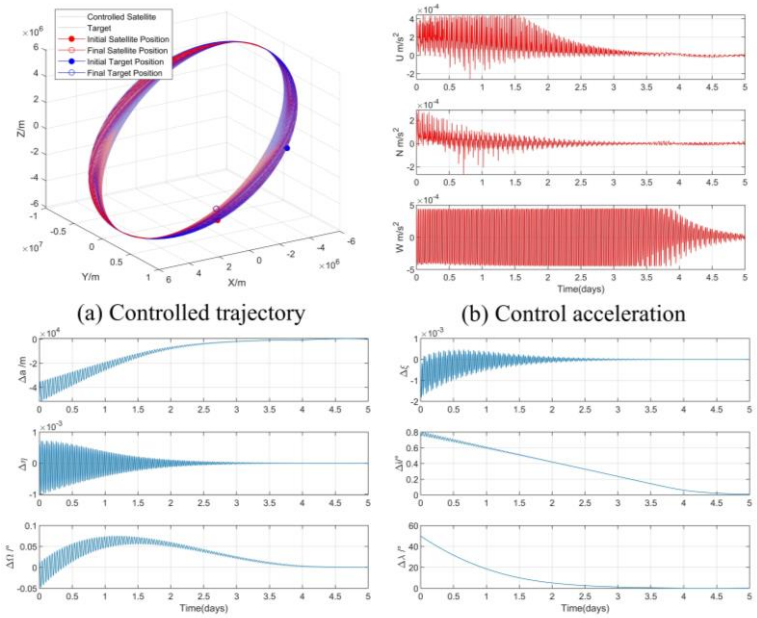

(a) Controlled trajectory (b) Control acceleration

(c) Control errors changing with time

Fig2 Single-satellite initialization results

3.2 Constellation reconfiguration for continuous coverage

A simulation for case of constellation reconfiguration for continuous coverage was carried out. Initial configuration is exhibited in Fig.3a. As shown in the figure, 10 satellites are evenly distributed on orbital plane 1 with orbit elements of $[a_1,e_1,i_1,\Omega_1,\omega_1]=[7528.14\text{km},10^{-4},53^{\circ},120^{\circ},0.01^{\circ}]$ at an interval of 36°, $M_1=[0^{\circ}:36^{\circ}:324^{\circ}]$. Another 10 satellites are 50km above at orbital plane 2, where a_2=7578.14km. The other orbit elements keep the same as for satellites in plane 1. Suppose an emergency occurs and continuous coverage is needed. All 10 satellites in orbital plane 1 is required to maneuver to plane 2 in one day using the proposed APF-based method. In the final state, the satellites are evenly spaced with an interval of 18° as presented in Fig.3b. The cone half angle of each satellite is θ=45°, illustration of the continuous coverage is presented in Fig.3c, with a maximum coverage bandwidth of 1300km. The maximum fuel consumption for a single satellite was 0.23kg.

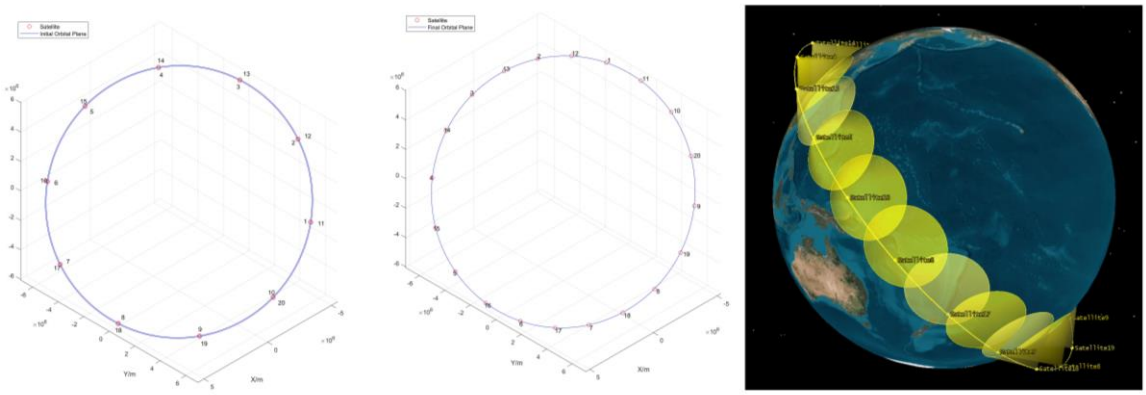

(a) Initial configuration (b) Final configuration (c) Continuous coverage result

Fig.3 Continuous coverage reconfiguration results

3.3 Constellation reconfiguration for simultaneous multipoint observation

Multipoint revisit requires a group of satellites with the same a and $e\approx 0$. Suppose ω_e is the earth rotation velocity, $\dot{\Omega}$ is the average changing rate of Ω due to J_2 perturbation , then the trajectories of successive adjacent satellites need to be distributed on the equatorial plane with an interval of $\Delta\alpha = T_N\left(\omega_e - \dot{\Omega}\right)$, where:

$$T_N \approx \left(\frac{2\pi}{n}\right)\left[1-\frac{3}{2}J_2\left(\frac{R_e}{a}\right)^2\left(3-\frac{5}{2}\sin^2 i\right)\right] \tag{19}$$

Let the ground track returns once after Q laps in N days, then the T_N needs to satisfy $D_N = 2\pi/\left(\omega_e - \dot{\Omega}\right), T_N = D_N/Q$. The successive adjacent satellites also need to have:

$$\frac{\Delta\Omega}{\omega_e} = -\frac{\Delta u}{n} \tag{20}$$

In this simulation case, an 18-satellite constellation was simulated with initial parameters of N=1, Q=15, e=10^{-4}, i=12.3°, a≈6878.14km, $\Delta\Omega = 20^\circ, \Delta u \approx \Delta\lambda \approx 55.61^\circ$, the max cone half angle θ=45° as shown in Fig.4a. Suppose a fire disaster occurs in Amazon Forest (0°N, 60°W), a severe flood occurs on Java Island (7°48’S, 110°18’E), a surveillance is needed above Huangyan Island (15°08’N, 117°48’E), an eruption from Kilauea Volcano occurs (19°26’N, 155°17’W) simultaneously. The coverage of the constellation requires to be extended, the inclination angle needs to be increased to i_t=15° while a, e, $\Delta\Omega, \Delta u$ remain unchanged for multipoint observation.

The constellation reconfiguration will need to be completed in 20 days. The final configuration is shown in Fig.4b and c. The variations of inclination i and the difference of Ω , λ between successive adjacent satellites with time is presented in Fig.4d, e and f. The maximum fuel consumption for a single satellite was 5.77kg. The average revisit time of the given locations can be seen in Table 1. After the reconfiguration, the Kilauea Volcano is included in the observation scope, the average revisit time of the Huangyan Island is reduced by half, while that of the Amazon Forest remains unchanged. The average revisit time of the Java Island is increased by 15min. In conclusion, simultaneous multipoint emergency observation constellation reconfiguration was accomplished by the proposed APF method.

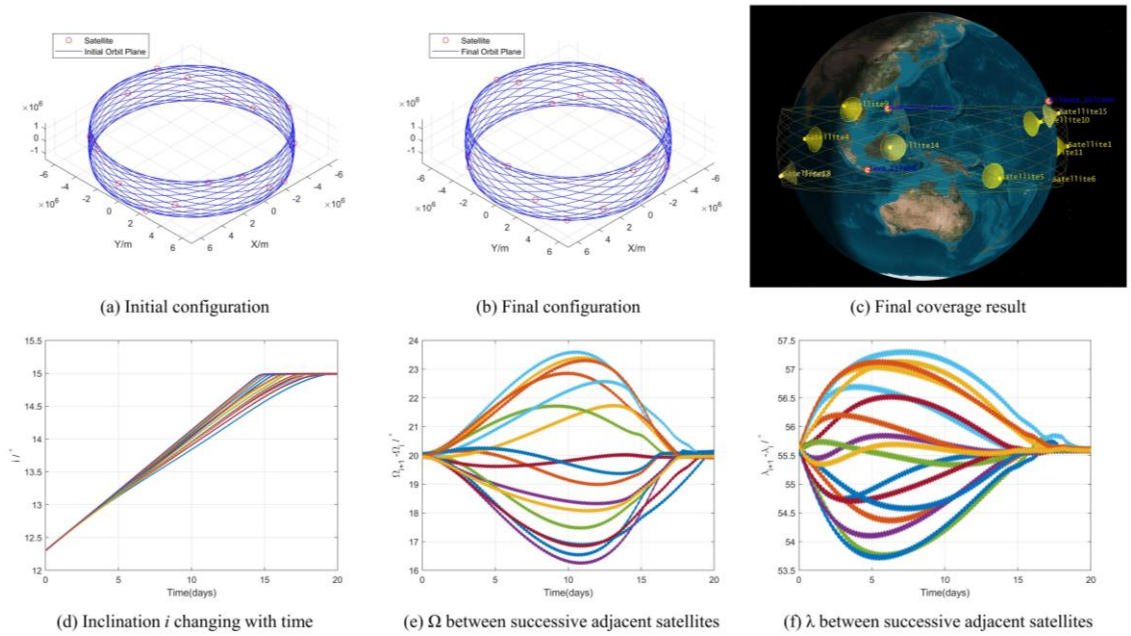

(a) Initial configuration (b) Final configuration (c) Final coverage result

(d) Inclination *i* changing with time (e) Ω between successive adjacent satellites (f) λ between successive adjacent satellites

Fig.4 Simultaneous multipoint observation reconfiguration results

Table 1 Average Revisit Time Results

	Average Revisit Time (Initial)	Average Revisit Time (Final)
Amazon Forest (0°N, 60°W)	20min	20min
Java Island (7°48'S, 110°18'E)	12min	27min
Huangyan Island (15°08'N, 117°48'E)	40min	20min
Kilauea Volcano (19°26'N, 155°17'W)	∞	76min

4. CONCLUSIONS

The proposed APF-based control method can be employed for constellation formation control and in the mission of simultaneous multipoint observation. Since the method is not complex and requires relatively low computational power, it may also be applied in a wide range of future applications.

5. REFERENCES

[1] Xu, Yun, Zhaokui Wang, and Yulin Zhang. "Bounded flight and collision avoidance control for satellite clusters using intersatellite flight bounds." *Aerospace Science and Technology* 94 (2019): 105425.

[2] Wang, Zhaokui, et al. "Self-organizing control for satellite clusters using artificial potential function in terms of relative orbital elements." *Aerospace Science and Technology* 84 (2019): 799-811.

[3] Xu, Yun& Wang, Zhaokui & Yulin, Zhang. (2021). Autonomous Continuous Low-Thrust Reconfiguration Control for Mega Constellations.

[4] Yu Y, Yue C, Li H, et al. Autonomous low-thrust control of long-distance satellite clusters using artificial potential function[J]. *The Journal of the Astronautical Sciences*, 2021, 68(1): 71-95.

[5] Lin, L., Jingshi, T.: Satellite Orbit Theory and Application, pp. 70–71. Publishing House of Electronics Industry Beijing, Beijing (2015)